Proceedings of ASME Turbo Expo 2017
GT2017
June 26-30, 2017, Charlotte, USA

GT2017-65153

NOVEL CURVATURE-BASED AIRFOIL PARAMETERIZATION FOR WIND TURBINE APPLICATION AND OPTIMIZATION

Karthik Balasubramanian*
Mark G. Turner
Kiran Siddappaji
Department of Aerospace Engineering
University of Cincinnati
Cincinnati, Ohio

ABSTRACT

The direct proportionality of streamline curvature to the pressure gradient normal to it causes the dependence of surface pressure loading on geometry curvature. This allows for the use of geometry curvature as a direct and aerodynamically meaningful interface to modify and improve performance of wind turbine sections. A novel blade parameterization technique driven by specification of meanline second derivative and a thickness distribution is presented. This technique is implemented as T-Blade3 which is an already existing in-house open-executable. The second derivative which is indicative of curvature, is used, enabling exploration of a large design space with minimal number of parameters due to the use of B-spline control points, capable of producing smooth curves with only a few points. New thickness and curvature control capabilities have been added to TBlade3 for isolated and wind turbine airfoils. The parameterization ensures curvature and slope of curvature continuity on the airfoil surface which are critical to smooth surface pressure distribution. Consequently, losses due to unintentional pressure spikes are minimized and likelihood of separation reduced. As a demonstration of the parameterization capability, Multi-Objective optimization is carried out to maximize wind turbine efficiency. This is achieved through an optimization tool-chain that minimizes a weighted sum of the drag-to-lift ratios over a range of angles of attack and sectional Reynolds numbers using a Genetic Algorithm. This allows for radial Reynolds number variation and ensures efficiency of wind turbine blade with twist incorporated. The tool-chain uses XFOIL to evaluate drag polars. This is implemented in MATLAB and Python in serial and in parallel with the US Department of Energy optimization system, DAKOTA. The Python and DAKOTA versions of the code are fully open-source. The NREL S809 horizontal axis wind turbine laminar-flow airfoil which is 21% thick has been used as a benchmark for comparison. Hence, the optimization is carried out with the same thickness-to-chord ratio. Drag coefficient improvement ranging from 17% to 55% for C_l between 0.3 and 1 was achieved.

Nomenclature

$\tilde{u}_i$	u coordinate of the ith control point
$\tilde{v}_i$	v coordinate of the ith control point
C	Streamline curvature
C_d	Sectional drag coefficient
C_l	Sectional lift coefficient
C_P	Power coefficient
C_p	Pressure coefficient
$C_{l,max}$	Maximum sectional lift coefficient
C_{l0}	Sectional lift coefficient at zero angle of attack
Cam	Total airfoil camber, difference between leading and trailing edge angles

*Address all correspondence to this author. Email: balasukt@mail.uc.edu

k	Scaling factor for camber line second derivative control points
n	Direction normal to streamine
ncp	Total number of control points
p	Pressure
R	Radius of streamline curvature
r	Local radius
r_{tip}	Tip radius
Re	Reynolds number
t	B-Spline parameter
thk	Airfoil thickness
u	Chord-wise coordinate in a chord normalized coordinate system
V	Velocity of the fluid
v	Coordinate perpendicular to chord in a chord normalized coordinate system

Greek Symbols

α	Airfoil angle of attack
χ	Airfoil Metal Angles

Subscripts

in	Condition at the leading edge
out	Condition at the trailing edge

Abbreviations

$2D$	Two dimensional
$3D$	Three dimensional
ASO	Aerodynamic Shape Optimization
$BEMT$	Blade Element Momentum Theory
CAD	Computer Aided Design
CER	Combined Experiment Rotor
CFD	Computational Fluid Dynamics
GA	Genetic algorithm
$HAWT$	Horizontal axis wind turbine
$MOGA$	Multi-objective genetic algorithm
$NREL$	National Renewable Energy Laboratory
SD	Second derivative

INTRODUCTION

Aerodynamic Shape Optimization (ASO) has been implemented and used to aid design for decades. Considerable research has been focused on optimization strategies which evolved with increase in computational speed and memory capacity and were applied to variable fidelity solvers. However, despite the ability of an optimizer to find a global optimum, the solution shape, and other shapes evaluated by the optimizer, are restricted by the scope and efficacy of the parameterization scheme. Corral and Pastor [1] observe that one of two different approaches can be used to parameterize an aerodynamic shape: Definition of the surface through discrete points, or through a series of curves. Samareh [2] reviews and compares nine different parameterization techniques that include Discrete points, Spline, CAD, Analytical and Free-Form Deformation approaches. The techniques are compared based on their abilities to produce smooth shapes and implement local control among other factors. Sripawadkul et al. [3] elucidates desirable characteristics of any parameterization technique and attempts quantitative comparison of five different schemes. The characteristics compared include Parsimony, Completeness, Orthogonality, Flawlessness and Intuitiveness. A parsimonious scheme allows for significant changes in geometry through minimal number of parameters, Completeness expresses ability of the scheme to describe any airfoil accurately, Orthogonality indicates that each shape produced corresponds to unique parameters, Flawlessness measures ability of the scheme to produce well-behaved shapes and Intuitiveness indicates the correspondence of the parameters directly to the geometry and physically meaningful changes.

B-splines have been widely implemented as parameterization schemes for ASO owing to the capability of local control and high degree of smoothness for complex geometries, devoid of oscillations that are characteristic of higher order polynomials. In this case, the coordinate locations of the B-spline control points constitute the parameters of optimization. The works of both Samareh [2] and Sripawadkul et al. [3] include the review of techniques that use B-spline control points to directly manipulate surface. This is also explored by Sobester and Barretty [4] who devise and examine a parsimonious B-spline scheme. Costanguay and Nadarajah [5] and Mousavi et al. [6] study the effect of parameterization on ASO by comparing different parameterization techniques and conclude that B-splines are suitable for drag minimization. Rashad and Zingg [7] and Giammichele et al. [8] have also exploited surface B-splines to optimize aerodynamic shape. Optimization of isolated airfoils specifically for wind turbine applications have also been focused on by a number of researchers [9, 10, 11]. Ritlop and Nadarajah [9] and He and Agarwal [11] have both presented redesigned optimized shapes based on the S809 wind turbine airfoil.

Curvature-Based Parametrization

The effect of surface curvature on the surface pressure distribution is a consequence of a fundamental fluid flow concept presented in Fox et al. [12]. This relation can be observed from Equation 1 which is the stream-wise application of Bernoulli's equation. The equation is reproduced here from Nemnem et al. [13]. The curvature is simply the reciprocal of the radius of curvature of the streamline.

$$\frac{1}{\rho}\frac{\partial p}{\partial n} = \frac{V^2}{R} = CV^2 \tag{1}$$

Korakianitis [14, 15] and Corral and Pastor [1] elucidate this theory and refer to available experimental and computational evidences, while observing that the pressure spikes that occur at the blending point between leading edge and blade due to curvature and slope-of-curvature discontinuities, are not detected easily in an experiment since it requires accurate probe placement and measurement resolution. The seminal works of Korakianitis [14, 15] emphasize that despite continuous surface curvature, discontinuities in slope-of-curvature, which is the case with most geometry generation techniques, causes kinks in pressure distribution in both cascades and isolated airfoils which result in local separation bubbles. This may also be observed if the leading edge is blended to the rest of the blade or isolated airfoil. More recently, experimental work of Shen et al. [16] investigates the effects of surface gradient-of-curvature discontinuities on the aerodynamic performance of Eppler 387 used in small wind turbines through wind tunnel experiments. The Eppler airfoil was redesigned by eliminating the discontinuities. They observe that such discontinuities cause a larger laminar separation bubble at lower angles of attack, resulting in higher drag. The redesigned airfoil also exhibits delayed stall. This work makes a strong case for the importance of surface curvature and slope-of-curvature by experimentally concluding that improved curvature distribution results in better aerodynamic performance. Other wind-turbine designers have incorporated curvature continuity for computational 2D wind turbine profile optimization [17, 18].

Going a step beyond ensuring curvature and slope-of-curvature continuity, specification of curvature can be used to construct the geometry, giving rise to curvature-based parameterization. This is a direct exploitation of the relationship between streamline curvature and surface pressure distribution. Korakianitis et al. [14, 19, 20, 21] present a method based on prescribing suction and pressure surface curvatures, and share motivations to the work presented in this paper. TBlade3, previously known as 3DBGB [22, 13], is a geometry generator that generates highly differentiable curves and surfaces for high performance turbomachinery 3D blades and cascade sections. The parameterization implemented by TBlade3 is based on superimposition of thickness distribution on a camber line. The generator ensures curvature and slope-of-curvature continuity, and uses specifications of the camber-line second derivative (SD) to construct a specified number of 2D sections, which are then stacked to form 3D blades, offering both chord-wise and smooth span-wise control. The camber-line SD is related to the camber-line curvature,

$$C = \frac{y''}{(1+y'^2)^{3/2}} \tag{2}$$

Both thickness and camber SD are parameterized through B-spline control points. Hence, smooth and complex curves can be obtained with only a few control points, indicating an inherently parsimonious scheme. Turner [23] clearly illustrates the intuitive manipulation of loading over a cascade blade by changes to the SD profile of the mean-line. TBlade3 has been used to create geometries for 3D optimization of turbomachinery. Mahmood et al. [24] presents optimization of a subsonic rotor. The optimized blade, produce by TBlade3, exhibits a complex and smooth 3D geometry with very few span-wise control points. Chen et al. [25] also performed optimization of a transonic rotor using TBlade3.

The existing tool required modification to incorporate construction of isolated wind turbine sections with a specified twist while retaining camber-line SD based parameterization. The modification implements the parameterization presented in this paper. A new thickness control is also implemented that encompasses the leading and trailing edge shapes, enabling exploration of a large design space of realistic smooth airfoils.

PARAMETERIZATION METHODOLOGY

The 2D section is generated in a chord-normalized (u-v) coordinate system with the leading edge at the origin. This is illustrated in Figure 1. The camber line is first constructed by integrating the specified SD values twice. A thickness distribution is then constructed in the same coordinate system and is superimposed onto the camber line. The thickness distribution and SD of the camber line are parameterized through Quartic and Cubic B-splines respectively with uniform knot vectors. This enables specification of the coordinate locations of the B-spline control points and the number of control points. The scheme implemented also requires the specification of other global parameters including maximum thickness-to-chord ratio, sectional twist angle, chord length, and total camber. The specified control points are first converted to smooth curves by using the parametric representation of a B-spline with uniform knots as presented by Nemnem et al. [13] for both Cubic and Quartic B-splines.

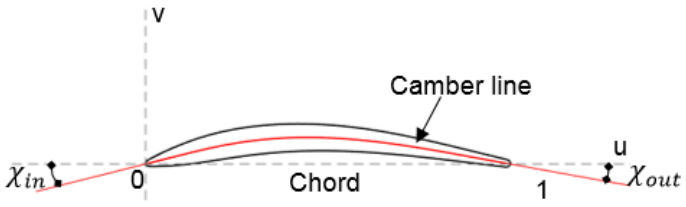

Figure 1. Generic airfoil profile illustrating inlet and exit blade metal angles.

Camber Line

The airfoil construction routine implemented by TBlade3 was formulated for turbomachinery blades, for which the exit

flow angles usually need to be held fixed. Hence, it was vital to have inlet and exit metal angles as parameters. These angles, along with the specification of mean-line SD were used to construct the camber line using an iterative implementation. The inlet and metal exit angles were enforced as boundary conditions during integration of slope of the camber line, and the value of stagger was also calculated along with the camber. This methodology is explained by Nemnem et al. [13]. However, for wind turbine applications, the values of inlet and exit metal angles lose their importance since the exit flow angle is of little consequence for analysis and optimization of an isolated airfoil, and the inlet flow angle for 2D cases is always axial. This would also be the case for wind turbine analyses involving a high pitch-length cascade. The differences between importance of parameters for a wind turbine and enclosed turbomachine necessitated the modification of camber line construction using more relevant parameters. Figure 1 presents a generic airfoil profile at zero angle of attack with inlet metal angle χ_{in} and exit metal angle χ_{out}.

The inlet and exit metal angles are related to the slopes of the camber line as follows,

$$v^{'}(0) = \tan\chi_{in} \tag{3}$$

$$v^{'}(1) = \tan\chi_{out} \tag{4}$$

The parameterization for an isolated section was reformulated to use a specification of the total overall camber instead of metal angles. Total camber is indicative of the zero lift angle of attack of an isolated airfoil. Higher total camber would require the airfoil to be at more negative angle of attack to produce zero lift. The blade can then be rotated by a specified angle of twist for subsequent construction of the 3D blade. The total overall camber can be expressed as $\chi_{out} - \chi_{in}$. The actual values of χ_{out} and χ_{in} are decided in the process by a combination of the total camber and SD specification. The slope of camber can be determined using Equation 5,

$$v^{'}(u) = k\int v^{''}(u)du + C_1 \tag{5}$$

where, k is a scaling factor that scales each SD specification in order to enforce the total camber as $\chi_{out} - \chi_{in}$. Hence, the designer specifying SD control points does not have to be concerned with their absolute values, only the relative values are of consequence. The analytical function $v^{''}(u)$ in the above equation is obtained as a smooth curve from the control point specification. Equation 5 is integrated again to determine the camber line coordinates, as expressed in Equation 6,

$$v(u) = k\iint v^{''}(u)du + C_1u + C_2 \tag{6}$$

where, $C_1$and C_2 are the constants of integration. The above equation contains three unknowns: k, $C_1$and C_2, which can be determined by applying the conditions in

$$v(0) = 0 \tag{7}$$

$$v(1) = 0 \tag{8}$$

$$\arctan v^{'}(1) - \arctan v^{'}(0) = Cam \tag{9}$$

where, Cam is the total camber, $Cam = \chi_{out} - \chi_{in}$

Applying the boundary condition in Equation 7 to Equation 6 results in $C_2 = 0$. Applying Equation 8 to Equation 6 results in a definite integral expression for C_1,

$$C_1 = -k\iint_0^1 v^{''}(u)du \tag{10}$$

Equation 10 is then substituted into Equation 5 so that the final boundary condition from Equation 9 can be applied,

$$v^{'}(0) = -k\iint_0^1 v^{''}(u)du \tag{11}$$

$$v^{'}(1) = k\left\{\int_0^1 v^{''}(u)du - \iint_0^1 v^{''}(u)du\right\} \tag{12}$$

Using Equations 3,4,9,11,12 and the trigonometric identity $\arctan u + \arctan v = \arctan\left({}^{u+v}/_{1-uv}\right)$,

$$Cam = \arctan\left\{\frac{k\iint_0^1 v^{''}(u)du}{1 - k^2 \cdot P}\right\} \tag{13}$$

where P is the definite integral evaluation,

$$P = \int_0^1 v''(u)du \cdot \iint_0^1 v''(u)du - \left(\iint_0^1 v''(u)du \right)^2 \tag{14}$$

All the integrals in the above equation are definite integrals and are evaluated through the analytical integration of B-splines with specified SD control points. Equation 13 is then recast as,

$$k^2 \cdot P\tan(Cam) + k \iint_0^1 v''(u)du - \tan(Cam) = 0 \tag{15}$$

Equation 14 is a quadratic equation in k and is solved as,

$$k = -\iint_0^1 v''(u)du \pm \frac{\sqrt{(\iint_0^1 v''(u)du)^2 + 4 \cdot P \cdot Cam^2}}{2 \cdot P \cdot Cam} \tag{16}$$

Equation 16 produces two roots and the appropriate value of k is chosen. The value of C_1 can be determined from Equation 10. The values of C_1 and k are then substituted in Equation 6 to obtain the camber line. The inlet and exit angles of the camber line can be known by evaluating Equations 11, 12 and applying them to Equations 3 and 4. The construction of camber line is complete and is rotated by the specified twist angle after superimposition of thickness.

Thickness Distribution

The thickness distribution along the chord of each 2D section is constructed using a parametric uniform Quartic B-spline. Hence, superposition of this thickness distribution curve onto the camber line results in curvature and slope-of-curvature continuity of the airfoil. The control points are specified as inputs. While the designer has sufficient local control by choosing the control points, the geometry generator is required to produce a thickness distribution that drops to zero at the leading and trailing edges to produce realistic streamline geometries. Due to the camber-thickness approach implemented here, the thickness above and below the camber line are symmetric by definition. Hence, the distribution derived from the control points are required to be symmetrically applied to the airfoil. While this approach inherently prevents negative thickness from occurring, conditions must be imposed to ensure smooth leading and trailing edges. The algorithm described here aims to impose these conditions, while ensuring sufficient freedom to the designer or optimizer. In order to achieve this, two control points are internally added to the beginning and end of the specified set of points, and are solved for. The values of these internally generated points depend on the specified thickness. A maximum thickness to chord ratio is then achieved based on the specified value, by simply multiplying the thickness distribution by an appropriate magnitude. Similar to the SD specification, this implies that the relative values of the control points are of importance, not the absolute values. The introduction of internally generated control points results in 8 unknowns: u and v coordinates of each of the four control points.

Enforcement of zero thickness at leading and trailing edges can be expressed as Equations 17 and 18 which is simply the evaluation of the first segment of a uniform B-spline at $t = 0$, where t is the B-spline parameter,

$$\frac{1}{24}\tilde{u}_1 + \frac{11}{24}\tilde{u}_2 + \frac{11}{24}\tilde{u}_3 + \frac{1}{24}\tilde{u}_4 = 0 \tag{17}$$

$$\frac{1}{24}\tilde{v}_1 + \frac{11}{24}\tilde{v}_2 + \frac{11}{24}\tilde{v}_3 + \frac{1}{24}\tilde{v}_4 = 0 \tag{18}$$

where $\tilde{u}_i$ and $\tilde{v}_i$ denote the chordwise locations and thickness control of the first four control points.

Equation 19 implies that the value of u-coordinate must be equal to 1 at the edge of the last segment which occurs when $t = 1$, while Equation 20 implies that the value of thickness at the edge of the last segment, which would be the trailing edge, must equal 0,

$$\frac{1}{24}\tilde{u}_{ncp} + \frac{11}{24}\tilde{u}_{ncp-1} + \frac{11}{24}\tilde{u}_{ncp-2} + \frac{1}{24}\tilde{u}_{ncp-3} = 1 \tag{19}$$

$$\frac{1}{24}\tilde{v}_{ncp} + \frac{11}{24}\tilde{v}_{ncp-1} + \frac{11}{24}\tilde{v}_{ncp-2} + \frac{1}{24}\tilde{v}_{ncp-3} = 0 \tag{20}$$

where ncp is the total number of control points.

Two more mathematical conditions were imposed to ensure smooth, blunt leading and trailing edges. Since the thickness is symmetrical about the camber line, smooth edges necessitate that $du/dthk = 0$ at the leading and trailing edge points. This leads to,

$$\frac{du}{dthk} = 0 \Longmapsto \frac{du}{dt} \cdot \frac{dt}{dthk} = 0 \Longmapsto \frac{du}{dt} = 0 \tag{21}$$

The above holds true at the leading and trailing edge points, and is the only possible condition since $dt/dthk$ cannot equal zero. This

is due to the requirement that the thickness should change in the vicinity of the leading and trailing edge points in order to drop to zero.

In order to satisfy the above, the B-spline coefficients are analytically differentiated and result in the following,

$$-\frac{1}{6}\tilde{u}_1 - \frac{1}{2}\tilde{u}_2 + \frac{1}{2}\tilde{u}_3 + \frac{1}{6}\tilde{u}_4 = 0 \tag{22}$$

$$-\frac{1}{6}\tilde{u}_{ncp} - \frac{1}{2}\tilde{u}_{ncp-1} + \frac{1}{2}\tilde{u}_{ncp-2} + \frac{1}{6}\tilde{u}_{ncp-3} = 0 \tag{23}$$

Equations 17 and 22 form a closed system and are easily solved to determine $\tilde{u}_1$ and $\tilde{u}_2$. Similarly, Equations 19 and 23 are solved to determine $\tilde{u}_{ncp}$ and $\tilde{u}_{ncp-1}$. Hence, 4 of the 8 unknowns are solved for. Since, only two more conditions of zero thickness at leading and trailing edge points are to be implemented, the values of $\tilde{v}_2$ and $\tilde{v}_{ncp-1}$ are allowed to be modified by the designer or optimizer while the values of $\tilde{v}_1$ and $\tilde{v}_{ncp}$ are determined by solving Equations 18 and 20 using the specified values of $\tilde{v}_2$ and v_{ncp-1}.

DEMONSTRATION OF CAPABILITY

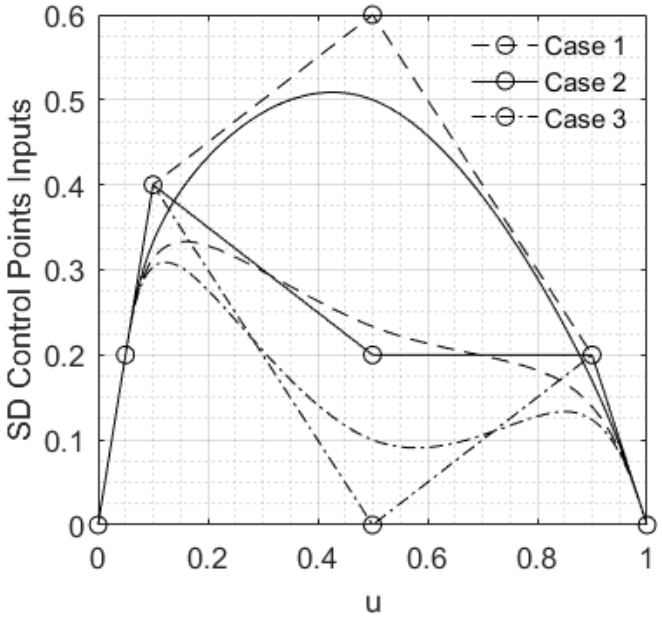

Figure 2. Incremental changes in second derivative control points.

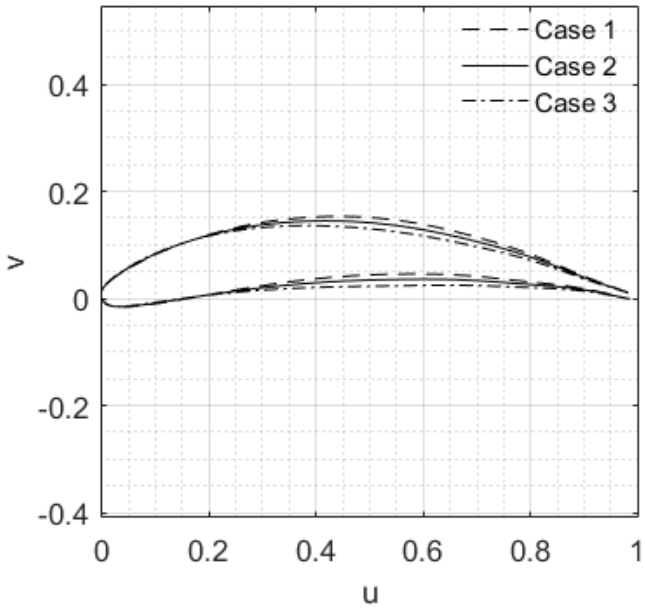

Figure 3. Airfoil shapes with truncated trailing edges.

The parameterization scheme described above is demonstrated here in order to further support and illustrate the advantages of using specification of camber-line SD. Generic camber SD and thickness distributions are used to generate an airfoil. Incremental changes are then made to a SD control point to create more geometries. The pressure distributions of the geometries are determined and plotted to highlight relation between the control points and flow.

XFOIL [26], which is the open-source implementation of a 2D panel method incorporating viscous/inviscid coupling, is used to generate the incompressible flow pressure coefficient distributions. The contour of the airfoil geometry is divided into a specified number of panels. The inviscid formulation superimposes vortex and source sheets on a freestream flow, and is coupled to a viscous formulation. For an incompressible flow, this formulation requires only the specification of Re and angle of attack. Equivalently, the required C_l can be specified instead of α, and the corresponding α is determined by XFOIL. The laminar-turbulent transition model formulates the growth of the Tollmien-Schlichting wave amplitude n and incorporates an e^n type amplification formulation to determine transition point. Analysis is carried out at a Reynolds number of $1 * 10^6$ and an angle of attack of 3°. The intuitiveness of the parameterization is also observed.

Figure 2 presents the SD control points which are specified. The peak control point in case 1 is the reduced from 0.6 to 0.2 and 0 to create two more cases. The actual SD curves obtained from the control points are also plotted in Figure 2. The airfoil shapes corresponding to each case is plotted in Figure 3. The re-

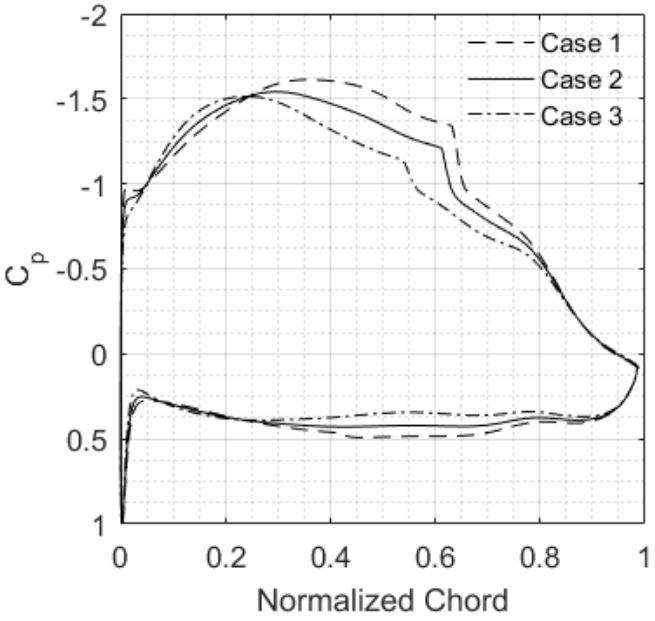

Figure 4. Coefficient of pressure distributions showing movement of peak suction.

lationship between the B-spline control and curve manipulation is clearly observed. Figure 4 displays the coefficient of pressure distribution for each of the three cases. As a consequence of the changes, the peak curvature shifts upstream for cases 2 and 3. The effect of this is further observed in Figure 4 as the peak suction location also shifts upstream from 36% chord in case 1 to 29% and 24% chord for cases 2 and 3 respectively. The direct correlation between the pressure distribution and SD control, which is indicative of curvature, allows for the use of aerodynamically relevant parameters and offers the designer vital insight of the flow before the CFD solver is used.

Wind Turbine Section Optimization

Motivation A wind turbine with a given radius ratio and power rating, experiences a range of local Reynolds number due to variation in local relative velocity and chord. Ge et al. [27] present this variation and showed that larger radius turbines experience local Reynolds numbers ranging almost an order of magnitude between 10^6 and 10^7. The effect of Reynolds number on aerodynamic performance of airfoils is presented by McMasters et al. [28] by showing the change in maximum possible lift to drag ratio for a smooth airfoil. The lift coefficient at maximum L/D also varies [27]. Airfoil L/D, in turn, limits the maximum achievable power coefficient as shown by Manwell et al. [29]. For any given tip speed ratio, the maximum C_P increases with L/D of the ideal blade airfoil [29]. Hence, local airfoil L/D changes with local Re and limits the C_P of the blade. Therefore, maximizing L/D of the local airfoil section is an integral part of achieving optimal power coefficient. The blade chord and twist angle also need to be designed such that the wind turbine power coefficient is optimal.

A unified in-house BEMT tool [30][31] has been developed to design initial blades for wind turbines, hydro-kinetic turbines and propellers which is connected to an optimizer. The tool incorporates the effect of Reynolds number by using C_l and C_d obtained from a lookup table of polars for a single chosen airfoil at the respective local Reynolds number and angle of attack while calculating the blade performance. The aim of the optimization process presented here is to create a database of optimized airfoils for appropriate maximum thickness-to-chord ratios that can be used by the BEMT tool. Each section would be optimized for maximum L/D at a specified range of Re and range of C_l. This would result in a wide envelope of optimal operating conditions corresponding to each airfoil. As part of the larger BEMT based optimization loop, the parameterization method provides a design space of high performance airfoils, which is then used by the BEMT tool to produce an optimal wind turbine blade.

The necessary framework to achieve this has been presented here and executed to produce a single airfoil and serves as a demonstration of the capabilities of the parameterization and its utility as part of wind turbine optimization.

Choice of Solver XFOIL is used as part of the optimizer tool-chain to evaluate aerodynamic properties of the geometry, the primary motivation being speed of evaluation with reasonable accuracy. XFOIL has been extensively used in the industry with multiple studies comparing with experimental measurements. Ronsten [32] compares wind tunnel static pressure measurements on a non-rotating horizontal axis wind turbine with XFOIL calculations and observes good agreement, especially for Re numbers higher than $5E5$ at all radial stations expect at the tip. Traub and Cooper [33] compare wind tunnel pressure distributions of a 16% thick S8036 airfoil profile at Reynolds numbers less than $2E5$ to XFOIL and observe good agreement for most cases. The most disagreement was observed in the location of the laminar separation bubble at low Re. Timmer and Van Rooij [34] present RFOIL, a modified version of XFOIL. A comparison is made between XFOIL, RFOIL and wind tunnel experimental data of the DU series airfoil profiles at a Re of $2E6$. RFOIL exhibited better prediction of $C_{l,max}$ and post stall characteristics. Although, the drag is underestimated, good agreement is observed between all three cases at lower lift coefficients. Ge et al. [27] show that the local Reynolds numbers for most commercial wind turbines ranging from 200kW to 6MW vary between $1E6$ and $1E7$, a range for which XFOIL has shown good agreement with experimental data. The optimization presented here considers a case with Reynolds numbers very close to

this range and for a range of C_l lower than $C_{l,max}$. These factors make XFOIL a suitable tool for the current case and is readily available.

Choice of Optimizer DAKOTA [35] is a freely available design analysis toolkit by Sandia National Laboratories and provides a framework for optimization, containing gradient-based, derivative-free methods and hybrid optimization capabilities. While many other robust optimizers are available, DAKOTA was chosen primarily for ease of integration with T-Blade3, zero cost and parallel capabilities. In order to optimize over a range of Re and Cl, a Multi-Objective Genetic Algorithm (MOGA) was used owing to the parallelized algorithm, capability to widely explore the entire design space available, and to be able to visualize the available optimal designs in the form of a Pareto front.

The underlying Genetic Algorithm (GA) is a population based numerical optimization strategy. It is well suited to explore design spaces that may contain frequent discontinuities, or if the calculation of objective function gradients are difficult. The design space is defined by the specification of minimum and maximum bounds on each parameter. In case of MOGA, an initial population is randomly chosen from the design space and the objective functions, or the fitness functions corresponding to each individual are assessed. The parameter sets with the worst fitness function values are eliminated. The remaining population is then modified through cross-over and mutation to produce the next generation of parameter sets. This is repeated and the GA eventually produces a population of non-dominated parameter sets. This would then form the Pareto front.

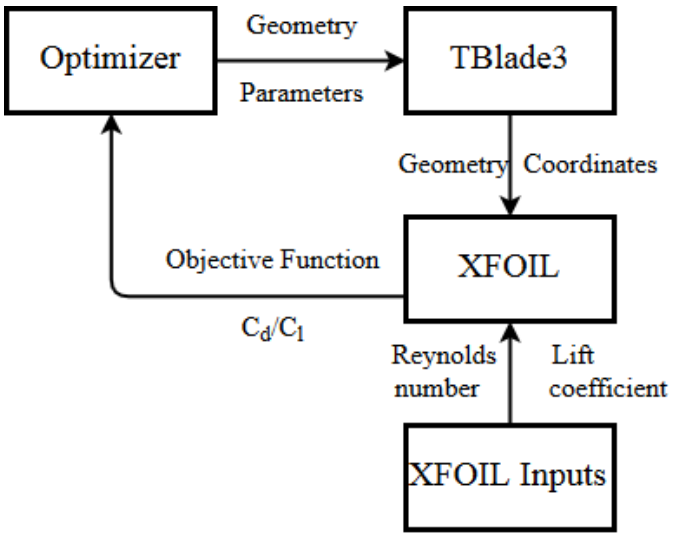

Figure 5. Flowchart of the optimization loop.

Optimization Ritlop and Nadarajah [9] and He and Agarwal [11] redesign the NREL S809 wind turbine airfoil through optimization. Successful optimization is carried out for a single point or a limited range of operation, as is the case with most studies currently in literature. The optimization presented in this paper attempts to produce an airfoil shape with better aerodynamic performance than S809 over a range of operating conditions while having an identical thickness-to-chord ratio.

The operating conditions of the Combined Experiment Rotor (CER) of the NREL [36] were used to calculate and choose Reynolds numbers for optimization. The CER is a three bladed rotor with a rated power of 20kW and operated at a constant 72 rpm. The maximum chord occurred at 25% which then tapered. Considering an airspeed range of 7m/s to 10m/s, it was calculated that about 25% to 60% of the blade experienced a Reynolds number that ranged between $7*10^5$ and $9.5*10^5$. The objectives were then chosen to be the unconstrained minimization of drag to lift ratios over a range of C_l values from 0.5 to 0.95 for two different Reynolds number, one at $7*10^5$ and another at $9.5*10^5$. The drag to lift ratios over a range of C_l values have been incorporated into the objective function in the form of a weighted average using Lagrangian multipliers. Hence, each objective function is a weighted average and corresponds to a single Reynolds number.

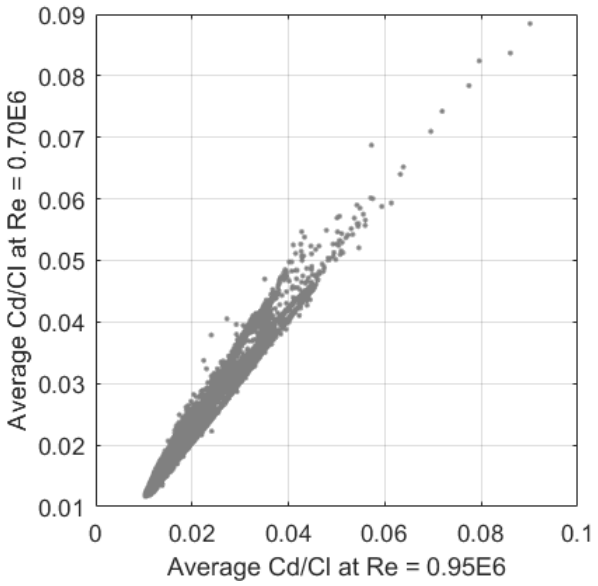

Figure 6. Function evaluations for average C_d/C_l at C_l = 0.5, 0.65, 0.8, 0.95.

The case presented in this paper does not bias the weight towards any single C_l and the weighted average reduces simply to an average. The values of C_l chosen for optimization are: 0.5,

0.65, 0.8 and 0.95. This range of C_l corresponds to a range of almost 5°of angles of attack for the S809. Thickness control points, camber SD control points, and total camber of the airfoil were used as parameters during optimization while the maximum thickness to chord ratio was held constant to a value of 21%. These values, while currently based on the NREL CER for purposes of demonstration, can be easily modified to meet the requirements of the larger BEMT optimization loop.

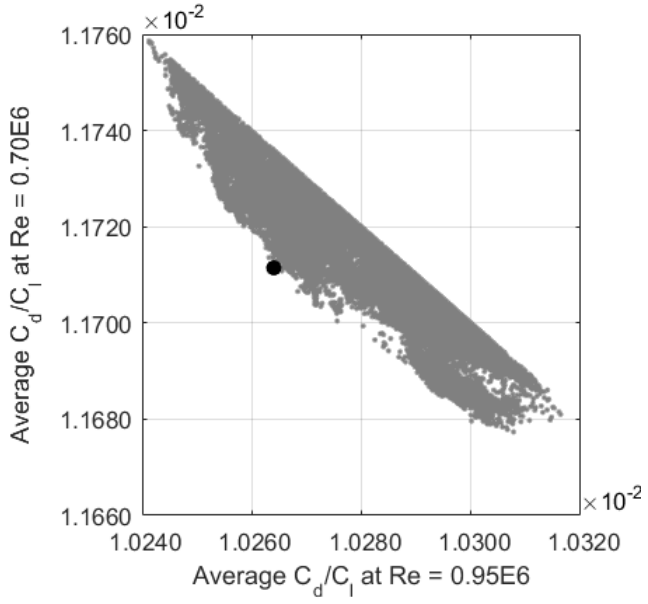

Figure 7. Pareto front for average C_d/C_l at C_l = 0.5, 0.65, 0.8, 0.95.

Successive executions of TBlade3 followed by XFOIL are required to evaluate the objective function from the input parametric values. Parallel optimization is achieved through DAKOTA. However, optimization tool-chains that utilize MATLAB and Python optimizers and execute in serial have also been scripted and are available. Figure 5 illustrates a schematic of the tool-chain created.

Results

The MOGA optimization resulted in a cloud of function evaluations as presented in Figure 6. Figure 7 was then created in order to display the Pareto front by restricting only those evaluations to appear, for which the sum of both the objective function values was less than a constant. The black dot in this figure shows the non-dominated design that was chosen as optimum from the Pareto front.

The optimized airfoil is presented in Figure 8. The SD, and thickness distributions are presented in Figures 9 and 10. The first and last two control points in Figure 10 are the internally generated control points. The optimization has produced an airfoil with relatively high overall camber of 24.3° with an inlet metal angle of 6.7° and exit metal angle of 17.6°.

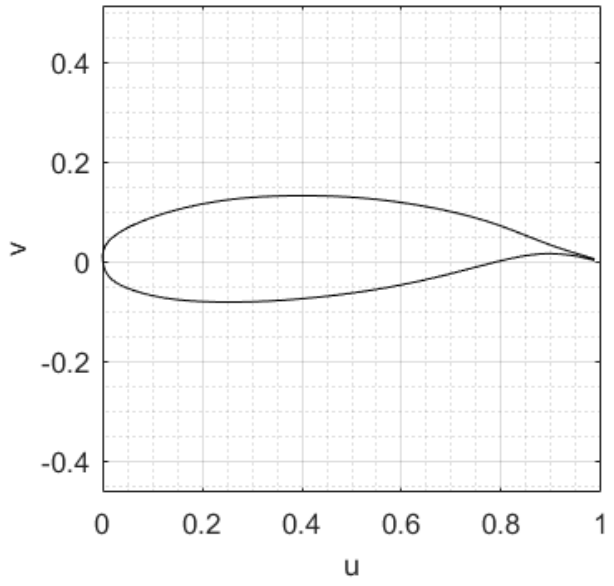

Figure 8. Optimum wind turbine profile.

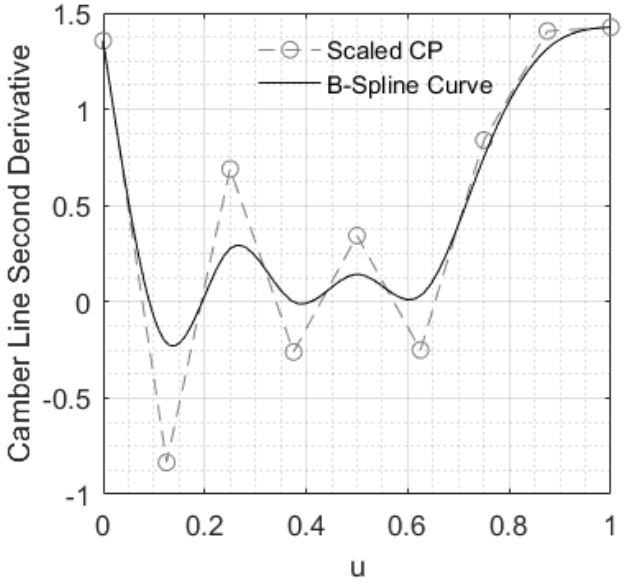

Figure 9. Camber line second derivative distribution for optimum airfoil.

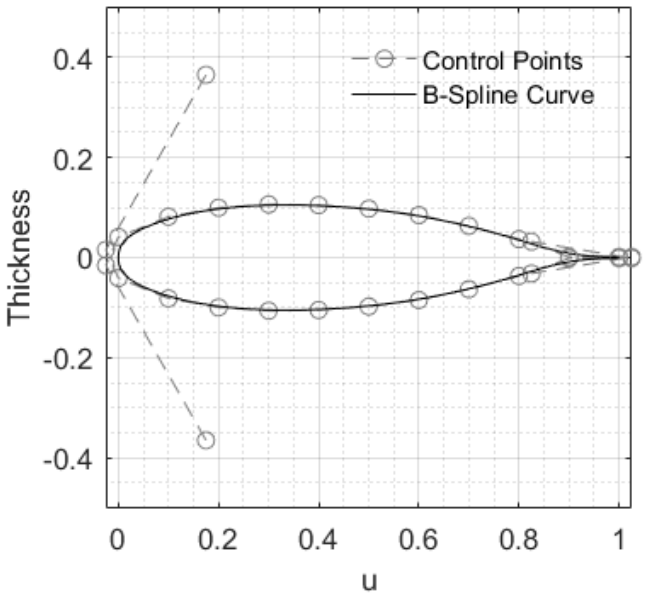

Figure 10. Thickness distribution for optimum airfoil showing control points specification.

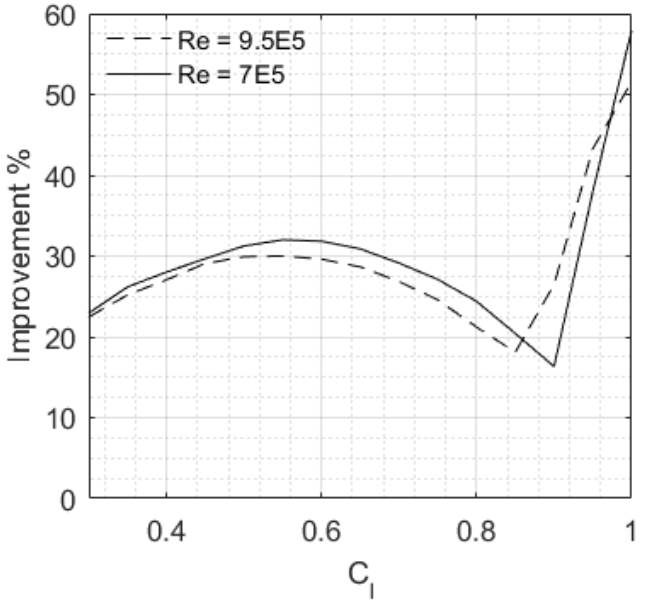

Figure 11. Improvement achieved by the optimized airfoil over S809 at different Re.

XFOIL analysis was carried out to analyze performance at all points of optimization and the optimized airfoil exhibited considerable improvement over S809. The high overall camber translates to a relatively high C_{l0}. Conversely, it produces C_l of 0 when at an α of -4.7° at $Re = 9.5 * 10^5$as opposed to a zero lift α of -1.3° for S809. A C_l value of 0.5 is achieved when the optimized airfoil is at an α of -0.1° while C_l of 0.95 is achieved at $\alpha = 2.7^\circ$. The improvement in aerodynamic performance is quantified as a percentage reduction in C_d using $(C_{d,S809} - C_{d,OPT})/C_{d,S809} * 100$. This quantity is calculated for C_l greater than 0.3 and is plotted in Figure 11 for both Reynolds numbers optimized for. Comparative plots of drag buckets for both airfoils are plotted in Figure 12 for both Reynolds numbers, and indicates that the optimized profile has a better performance over the entire range of positive C_l values while the optimization was carried out only for a subset of this range.

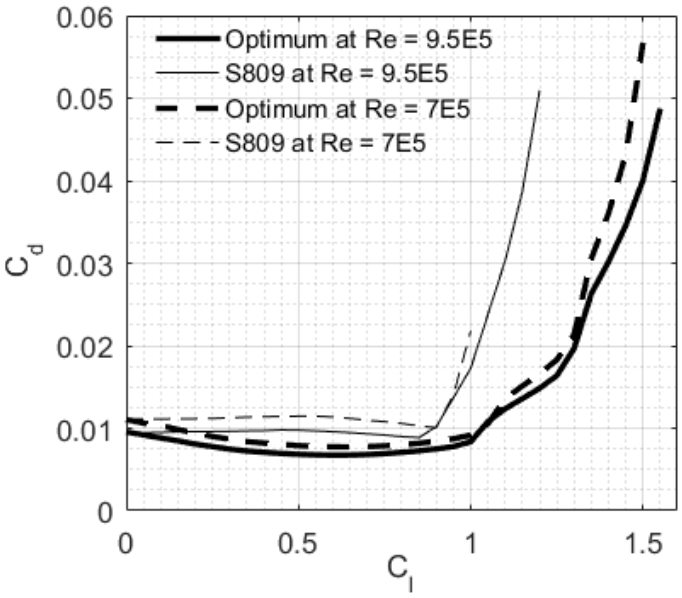

Figure 12. Comparison of drag buckets of optimized and S809 sections at different Re.

Pressure coefficient distributions for $Re = 9.5 * 10^5$ and a C_l value of 0.95 is plotted in Figure 13. It is observed that the thick leading edge of the airfoil does not exhibit the characteristic pressure spike at higher C_l unlike the S809. At lower C_l, the leading edge is less loaded owing to negative angle of attack which causes flow over the airfoil to experience very little camber near the leading edge. This characteristic behavior is also observed for $Re = 7.0 * 10^5$. The optimized airfoil also exhibits smooth pressure variations, devoid of any unintentional pressure spikes throughout the surface. The flow stays laminar longer than

S809 on both surfaces and stall is delayed. Figure 14 presents a comparison of the variation of C_l with α for S809 and the optimized airfoil and Figure 15 highlights the improvement gained in L/D over the range of Reynolds numbers optimized for.

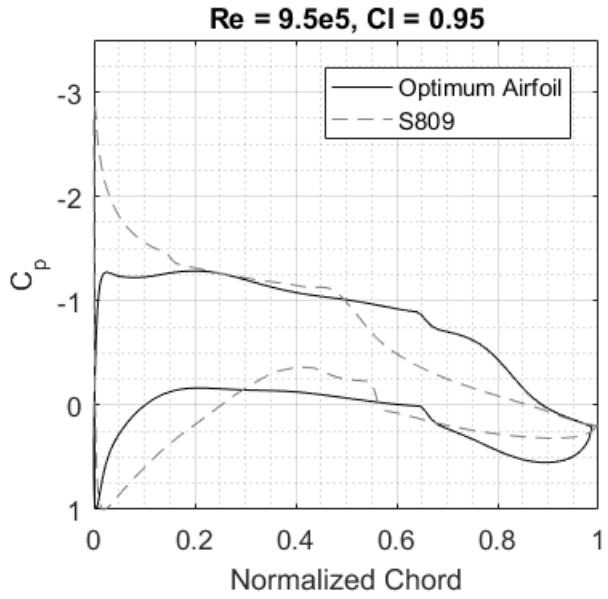

Figure 13. Comparison of pressure distributions for optimized and S809 sections at C_l = 0.95.

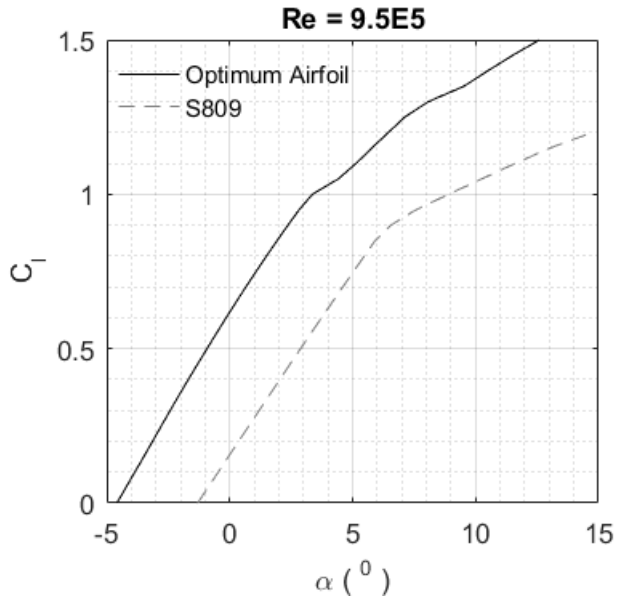

Figure 14. Comparison of $C_l - \alpha$ curve for S809 and optimized airfoil.

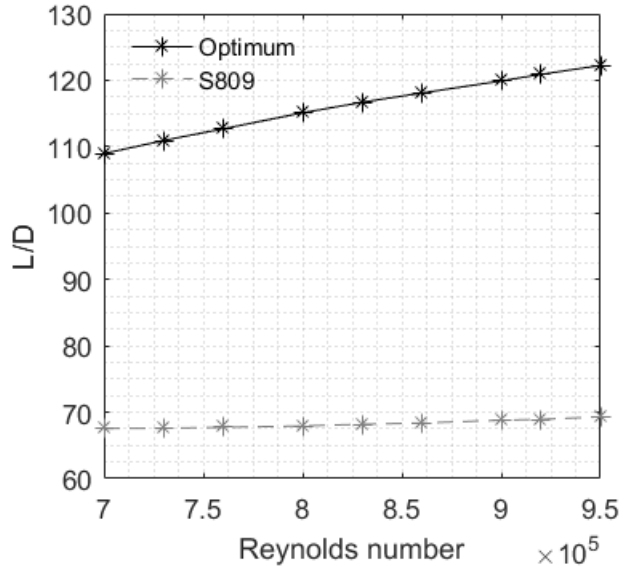

Figure 15. Lift-to-drag ratios for the range of Reynolds numbers optimized.

Other Capabilities

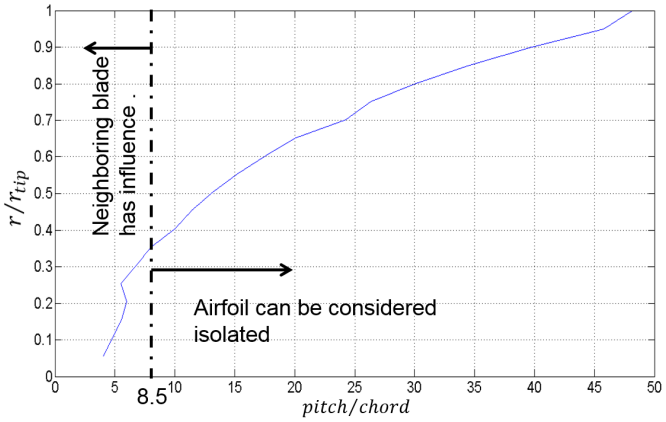

Figure 16. Region of blade to blade dependence as a function of radius and pitch-to-chord ratios. [37]

The capability of the parameterization presented here to incorporate a specified local airfoil twist allows for section optimization based on analysis of airfoil cascades. Dey [37] shows that the effect of neighboring blades in a wind turbine is a function of radius ratio and pitch-to-chord ratio. This is illustrated in Figure 16 reproduced here. It can be observed that at lower radii

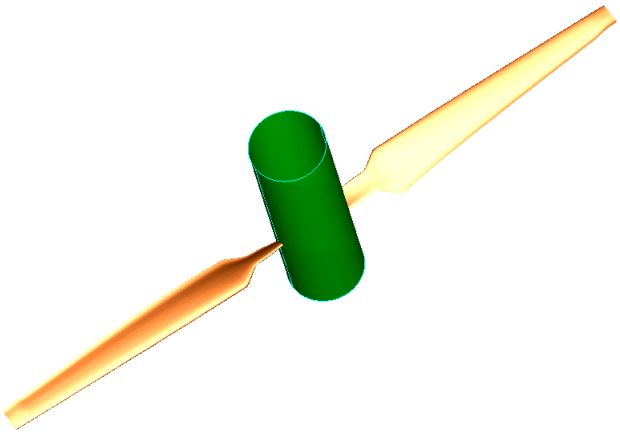

Figure 17. Wind turbine blade constructed from the optimized section using TBade3.

and higher chord lengths, the aerodynamics of the local section is affected by the neighboring blades. The specified twist can then be used to produce a staggered airfoil geometry. MISES [38] is a fast quasi three dimensional cascade analysis tool and can be used to analyze the staggered airfoil as a cascade. This set up can then be used to form an optimization tool-chain in a framework very similar to the one presented here with the purpose of providing optimized sections at lower radii to the BMET optimization tool-chain.

The 3D capabilities of TBlade3 have been utilized to create a wind turbine blade using the optimized airfoil produced with a specified twist distribution. This is presented in Figure 17. The current parameterization capabilities of TBlade3 allows for optimization of radial twist, taper, lean and sweep apart from sectional optimization.

CONCLUSIONS & FUTURE WORK

A novel parameterization technique for wind turbine and isolated airfoil sections based on camber line curvature is presented. The technique is implemented through modification of an existing in-house 3D geometry generator TBlade3 which has already been applied to generation and optimization of turbomachinery blades. The direct influence of curvature on the surface pressure distribution is taken advantage of through this parameterization. Camber line second derivative is used instead of curvature for linearity. B-spline control points are used for specifications of camber line second derivative from which camber line is constructed, and thickness, enabling complex variations with only a few design parameters. The scheme ensures curvature and slope-of-curvature continuity of the section. As a demonstration of capability, Multi-Objective optimization using Genetic Algorithm of an isolated airfoil for a thickness-to-chord ratio of 21% is performed over a range of C_l including 0.5, 0.65, 0.8 and 0.95 and Reynolds numbers of $7 * 10^5$and $9.5 * 10^5$.The NREL S809 HAWT airfoil is used as a benchmark for performance analysis. A non-dominated shape is chosen from the obtained Pareto front and it is observed that the pressure distribution over the section produced by TBade3 is smooth, and does not exhibit any unintentional spikes or dips. The optimized shape exhibits relatively high total camber of 24.3° and a thick leading edge. Considerable improvement ranging from 17% to 55% are achieved for lift coefficient values above 0.3, for both Reynolds numbers.

The optimization of isolated airfoils is easily extended to the optimization of an airfoil cascade for lower radii through a single rotation of the airfoil to achieve the desired twist angle. The existing capabilities of TBlade3 enables construction of 3D wind turbine blades through specification of multiple 2D sections, and specification of radial variation of parameters including twist, taper, lean and sweep. The radial parameters also use B-splines which can produce complex shapes with few parameters. This paves the way for 3D optimization of wind turbine blades.

REFERENCES

[1] Corral, R., and Pastor, G., 2004. "Parametric design of turbomachinery airfoils using highly differentiable splines". *Journal of Propulsion and Power,* **20**(2), pp. 335–343.

[2] Samareh, J., 2001. "Survey of shape parameterization techniques for high-fidelity multidisciplinary shape optimization". *AIAA Journal,* **39**(5), pp. 877–884.

[3] Sripawadkul, V., Padulo, M., and Guenov, M., 2010. "A comparison of airfoil shape parameterization techniques for early design optimization". In 13th AIAA/ISSMO Multidisciplinary Analysis and Optimization Conference 2010.

[4] Sobester, A., and Barretty, T., 2008. "The quest for a truly parsimonious airfoil parameterization scheme". In 8th AIAA Aviation Technology, Integration and Operations (ATIO) Conference.

[5] Castonguay, P., and Nadarajah, S., 2007. "Effect of shape parameterization on aerodynamic shape optimization". In Collection of Technical Papers - 45th AIAA Aerospace Sciences Meeting, Vol. 1, pp. 561–580.

[6] Mousavi, A., Castonguay, P., and Nadarajah, S., 2007. "Survey of shape parameterization techniques and its effect on three-dimensional aerodynamic shape optimization". In Collection of Technical Papers - 18th AIAA Computational Fluid Dynamics Conference, Vol. 1, pp. 234–254.

[7] Rashad, R., and Zingg, D., 2016. "Aerodynamic shape optimization for natural laminar flow using a discrete-adjoint approach". *AIAA Journal,* **54**(11), pp. 3321–3337.

[8] Giammichele, N., Trepanier, J.-Y., and Tribes, C., 2007. "Airfoil generation and optimization using multiresolution b-spline control with geometrical constraints". In Collection of Technical Papers - AIAA/ASME/ASCE/AHS/ASC

Structures, Structural Dynamics and Materials Conference, Vol. 3, pp. 2634–2644.

[9] Ritlop, R., and Nadarajahy, S., 2009. "Design of wind turbine profiles via a preconditioned adjoint-based aerodynamic shape optimization". In 47th AIAA Aerospace Sciences Meeting including the New Horizons Forum and Aerospace Exposition.

[10] Ram, K., Lal, S., and Rafiuddin Ahmed, M., 2013. "Low reynolds number airfoil optimization for wind turbine applications using genetic algorithm". *Journal of Renewable and Sustainable Energy,* **5**(5).

[11] He, Y., and Agarwal, R., 2014. "Shape optimization of nrel s809 airfoil for wind turbine blades using a multiobjective genetic algorithm". *International Journal of Aerospace Engineering,* **2014**.

[12] Fox, R. W., Pritchard, P. J., and McDonald, A. T., 2009. *Introduction to Fluid Mechanics*, seventh ed. John Wiley & Sons, Inc.

[13] Nemnem, A., Turner, M., Siddappaji, K., and Galbraith, M., 2014. "A smooth curvature-defined meanline section option for a general turbomachinery geometry generator". In Proceedings of the ASME Turbo Expo, Vol. 2B.

[14] Korakianitis, T., 1992. "Prescribed-curvature-distribution airfoils for the preliminary geometric design of axial-turbomachinery cascades". In ASME 1992 International Gas Turbine and Aeroengine Congress and Exposition, GT 1992, Vol. 1.

[15] Korakianitis, T., and Papagiannidis, P., 1992. "Surface-curvature-distribution effects on turbine-cascade performance". In ASME 1992 International Gas Turbine and Aeroengine Congress and Exposition, GT 1992, Vol. 1.

[16] Shen, X., Avital, E., Paul, G., Rezaienia, M., Wen, P., and Korakianitis, T., 2016. "Experimental study of surface curvature effects on aerodynamic performance of a low reynolds number airfoil for use in small wind turbines". *Journal of Renewable and Sustainable Energy,* **8**(5).

[17] Chen, J., Wang, Q., Pang, X., Li, S., and Guo, X., 2013. "Improvement of airfoil design using smooth curvature technique". *Renewable Energy,* **51**, pp. 426–435.

[18] Wang, Q., Wang, J., Sun, J., Ren, J., and Wei, Q., 2016. "Optimal design of wind turbine airfoils based on functional integral and curvature smooth continuous theory". *Aerospace Science and Technology,* **55**, pp. 34–42.

[19] Korakianitis, T., Rezaienia, M., Hamakhan, I., Avital, E., and Williams, J., 2012. "Aerodynamic improvements of wind-turbine airfoil geometries with the prescribed surface curvature distribution blade design (circle) method". *Journal of Engineering for Gas Turbines and Power,* **134**(8).

[20] Korakianitis, T., Hamakhan, I., Rezaienia, M., Wheeler, A., Avital, E., and Williams, J., 2012. "Design of high-efficiency turbomachinery blades for energy conversion devices with the three-dimensional prescribed surface curvature distribution blade design (circle) method". *Applied Energy,* **89**(1), pp. 215–227.

[21] Korakianitis, T., Rezaienia, M., Hamakhan, I., and Wheeler, A., 2013. "Two- and three-dimensional prescribed surface curvature distribution blade design (circle) method for the design of high efficiency turbines, compressors, and isolated airfoils". *Journal of Turbomachinery,* **135**(3).

[22] Siddappaji, K., Turner, M., and Merchant, A., 2012. "General capability of parametric 3d blade design tool for turbomachinery". In Proceedings of the ASME Turbo Expo, Vol. 8, pp. 2331–2344.

[23] Turner, M., 2017. "The role of curvature in turbomachinery design". In Global Power and Propulsion Forum 2017, no. 142.

[24] Mahmood, S., Turner, M., and Siddappaji, K., 2016. "Flow characteristics of an optimized axial compressor rotor using smooth design parameters". In Proceedings of the ASME Turbo Expo, Vol. 2C-2016.

[25] Chen, H., Turner, M., Siddappaji, K., and Mahmood, S., 2016. "Vorticity dynamics based flow diagnosis for a 1.5-stage high pressure compressor with an optimized transonic rotor". In Proceedings of the ASME Turbo Expo, Vol. 2A-2016.

[26] Drela, M., 1989. *XFOIL: An Analysis and Design System for Low Reynolds Number Airfoils*. Springer Berlin Heidelberg, Berlin, Heidelberg, pp. 1–12.

[27] Ge, M., Tian, D., and Deng, Y., 2016. "Reynolds number effect on the optimization of a wind turbine blade for maximum aerodynamic efficiency". *Journal of Energy Engineering,* **142**.

[28] Mcmasters, J. H., and Henderson, M. L., 1979. Low-speed single-element airfoil synthesis. Tech. rep., NASA, Langley Research Center.

[29] Manwell, J. F., McGowan, J. G., and Rogers, A. L., 2009. *Wind Energy Explained*, 2nd ed. Wiley.

[30] Siddappaji, K., and Turner, M. G., 2015. "Revolutionary geometries of mobile hydrokinetic turbines for wind energy applications". In Proceedings of ASME Turbo Expo, no. GT2015-42342.

[31] Siddappaji, K., and Turner, M. G., 2015. "Counter rotating propeller design using blade element momentum theory". In Proceedings of The International Conference on Airbreathing Engines, no. ISABE-2015-20196.

[32] Ronsten, G., 1992. "Static pressure measurements on a rotating and a non-rotating 2.375 m wind turbine blade. comparison with 2d calculations". *Journal of Wind Engineering and Industrial Aerodynamics,* **39**(1-3), pp. 105–118.

[33] Traub, L., and Cooper, E., 2008. "Experimental investigation of pressure measurement and airfoil characteristics at low reynolds numbers". *Journal of Aircraft,* **45**(4), pp. 1322–1333.

[34] Timmer, W., and Van Rooij, R., 2003. "Summary of the delft university wind turbine dedicated airfoils". pp. 11–21.

[35] Eldred, M. S., Adams, B. M., Haskell, K., Bohnhoff, W. J., Eddy, J. P., Gay, D. M., Hart, W. E., Hough, P. D., Kolda, T. G., Swiler, L. P., and Watson, J., 2008. *DAKOTA Reference Manual*, 4.2 ed. Sandia National Laboratories, Albuquerque, NM, November.

[36] Giguere, P., and Selig, M., 1999. Design of a tapered and twisted blade for the nrel combined experiment rotor. Technical Report NREL/SR-500-26173, NREL (National Renewable Energy Laboratory), Golden, CO, March.

[37] Dey, S., 2011. "Wind turbine blade design system, aerodynamic and structural analysis". Master's thesis, University of Cincinnati, Cincinnati, OH, May.

[38] Drela, M., and Youngren, H., 1998. *A User Guide for MISES 2.53*. MIT Computational Science Laboratory, December.